RSC Advances

PAPER

View Article Online
View Journal | View Issue

Cite this: *RSC Adv.*, 2017, **7**, 11414

Room temperature methane sensing properties of α-$Fe_{2-x}Cu_xO_3$ nanoparticles

Haifeng Liu,*[a] Tongjiang Peng,[ab] Hongjuan Sun,[b] Ruishi Xie[a] and Guohua Ma[a]

Received 2nd November 2016
Accepted 1st February 2017

DOI: 10.1039/c6ra26167a

rsc.li/rsc-advances

α-$Fe_{2-x}Cu_xO_3$ ($0 \leq x \leq 0.17$) nanoparticles were synthesized using an improved homogenous co-precipitation method. The effects of doped Cu on crystal structure of α-Fe_2O_3 were investigated by field emission transmission electron microscopy, X-ray diffraction and Raman spectroscopy. Owing to the substitution of Cu^{2+} at the Fe^{3+} sites, the lattice parameters of α-$Fe_{2-x}Cu_xO_3$ with an average particle size of ~40 nm and a single corundum structure increased with increasing doped Cu concentration. The shifting of Raman peaks for α-$Fe_{2-x}Cu_xO_3$ to higher wavenumber was also observed due to the strong electron–phonon interactions and structural distortion after doping Cu. According to the conductivity measurements, doping Cu can increase the concentration of hole carriers and enhance the conductivity of the p-type α-Fe_2O_3 semiconductor. Furthermore, CH_4 sensing characterization showed that the α-$Fe_{2-x}Cu_xO_3$ nanoparticles are sensitive and have a good selectivity to CH_4 at room temperature, and the response of the material is evidently improved by doping with Cu. The maximum response to 2000 ppm CH_4 at room temperature and 50% relative humidity was obtained when $x \approx 0.10$, meeting the common requirements in application. These results suggest that α-$Fe_{2-x}Cu_xO_3$ nanoparticles can be considered a potential candidate for methane detection at room temperature.

1. Introduction

Methane (CH_4), the second potent greenhouse gas, is often found in environment, industrial and domestic areas.[1–3] It is the major component of natural gas, which is used widely in industries, automobiles and homes. However, it is necessary to detect CH_4 from coal mines, factories, farmland ventilation or natural gas-fueled appliances because it can form an explosive mixture in air if its concentration is in the range of 5–15%. There are several traditional techniques for CH_4 detection, such as gas chromatography equipped with a flame ionization detector (GC-FID)[4,5] or infrared spectral radiometry.[6] However, these common measurement methods for CH_4 have some disadvantages, requiring high cost equipment and strict working conditions. In the past few decades, metal-oxide semiconductors, such as SnO_2,[2] α-Fe_2O_3,[7] and ZnO,[8] have been investigated widely as CH_4 sensing materials because of their high response and simplicity in synthesis. Although these metal-oxide semiconductors have more advantages for CH_4 detection, there are also some problems including their low selectivity, particularly high working temperature (about 400–500 °C). The identification of CH_4 at temperatures lower than 350 °C is relatively difficult owing to its high thermodynamic stability compared to that of other hydrocarbons.[3] High working temperature in an atmosphere containing CH_4 is dangerous and may result in an explosion. Hence, there is strong demand for a reliable sensor that can detect CH_4 at or near room temperature. Nowadays, much effort has been devoted to reduce the gas-sensing temperature of metal oxides. For example, materials, such as Pd and Pt, catalyzing CH_4 decomposition at a relatively low temperature of 300 °C are loaded mainly in the stable metal oxides.[2,9] Unfortunately, the loading of noble metals has high cost and causes environmental pollution. Recently, great emphasis is being given on nano-structured[4,10] and doped metal[11] oxides as sensor materials to reduce the gas-sensing temperature. Nevertheless, the operating temperature of the vast majority of CH_4 sensors is not room temperature, and further studies are still necessary.

As a result, in the present study, α-$Fe_{2-x}Cu_xO_3$ nanoparticles were selected and synthesized by an improved homogenous co-precipitation method. Based on the characteristics for the morphology, crystal structure and electric conductivity, the effects of doped Cu on crystal structure distortion and semiconducting property were investigated. The CH_4 sensing properties of the α-$Fe_{2-x}Cu_xO_3$ nanoparticles were then examined. As expected, the sensor using α-$Fe_{2-x}Cu_xO_3$ nanoparticles as a gas sensing material exhibited a receivable response to CH_4 at room temperature.

2. Experimental

All the chemical reagents were analytically pure without further purification. α-$Fe_{2-x}Cu_xO_3$ nanoparticles were prepared by an

[a]*Analytical and Testing Center, Southwest University of Science and Technology, Mianyang 621010, PR China. E-mail: haifengliu2010@hotmail.com; Fax: +86 816 6089508; Tel: +86 816 6089509*

[b]*Institute of Mineral Materials & Application, Southwest University of Science and Technology, Mianyang 621010, PR China*

Table 1 Mol ratio of $n(Cu^{2+})/n(Fe^{3+})$ for preparing the hydroxide of α-$Fe_{2-x}Cu_xO_3$ nanoparticles

Sample ID	Value of x	$n(Cu^{2+})/n(Fe^{3+})$	Sample ID	Value of x	$n(Cu^{2+})/n(Fe^{3+})$
CF-0	0	0	CF-5	0.10	0.05
CF-1	0.02	0.01	CF-6	0.11	0.06
CF-2	0.04	0.02	CF-7	0.13	0.07
CF-3	0.06	0.03	CF-8	0.15	0.08
CF-4	0.08	0.04	CF-9	0.17	0.09

improved homogenous co-precipitation method. First, $FeCl_3 \cdot 6H_2O$ and $CuCl_2 \cdot 2H_2O$ were mixed and dissolved with different mol ratios of $n(Cu^{2+})/n(Fe^{3+})$ at a given constant Fe^{3+} concentration of 0.10 mol L^{-1} (shown in Table 1), which was marked as solution A. Ammonia was diluted five times with distilled water according to the volume ratio, marked as solution B. Solutions A and B were dropped slowly into a distilled water reaction medium, in which sodium stearate was used as the dispersing agent. During the reaction, the reaction medium was stirred by a magnetic stirring apparatus at 20 °C, and the dropping speeds of solutions A and B were controlled at a certain ratio to maintain the pH value of the entire system at about 3. The formed precipitates were centrifugally separated, washed, heated at 60 °C for 10 h, and then annealed at 300 °C in an oxygen atmosphere for 1 h.

Subsequently, α-$Fe_{2-x}Cu_xO_3$ gas sensors were fabricated as follows. The prepared α-$Fe_{2-x}Cu_xO_3$ nanoparticles were mixed with the solution of polyvinyl alcohol to form a paste, which was coated onto the α-Al_2O_3 ceramic sheets (22 mm in length, 4 mm in width, attached with a pair of Ag electrodes and shown as Fig. 1a) using a small brush to form a film with a thickness of around 0.5 mm.

The morphology and crystallization of the α-$Fe_{2-x}Cu_xO_3$ nanoparticles were observed using a FEI Tecnai G2 F20 field emission transmission electron microscope (TEM) with an acceleration voltage of 200 kV. The structural characterization was performed using a PANalytical X' Pert PRO X-ray diffractometer (XRD) with Cu $K_{\alpha 1}$ radiation (λ = 0.15406 nm). The vibrational modes and structural distortion of the α-$Fe_{2-x}Cu_xO_3$ nanoparticles were investigated using a Renishaw inVia confocal microprobe Raman spectroscopy with the laser excitation of 785 nm, which provided a power at the sample surface of ~1.7 mW and was focused through the 50× objective to a 1–2 μm spot, at room temperature. The electrical property of the α-$Fe_{2-x}Cu_xO_3$ gas sensors was measured using a two probe technique. The gas sensing experiments were carried out using a static testing method.[12] The schematic of the equipment for sensor resistance measurement is shown in Fig. 1b. The response of the sensor was determined by the resistance ratio of sensor device in clean air (R_a) and in an atmosphere containing test gas (R_g), *i.e.*, the sensor response $S = R_a/R_g$. The value of R_a and R_g can be obtained by measuring the voltage on the load resistance R_L.

3. Results and discussion

3.1. Morphological characteristics of the α-$Fe_{2-x}Cu_xO_3$ nanoparticles

Fig. 2 presents FE-TEM images of α-$Fe_{2-x}Cu_xO_3$ nanoparticles. Part (a) and (b) show the bright field TEM image and high resolution TEM (HRTEM) image of undoped α-Fe_2O_3 grains, whereas parts (c) and (d) provide the bright field TEM image and HRTEM image of α-$Fe_{1.92}Cu_{0.08}O_3$, respectively. Fig. 2a shows that the undoped α-Fe_2O_3 powder consists of irregular particles with sizes in the range from 20 to 80 nm. To obtain more detailed structural information, a corresponding HRTEM image was recorded on the edge of the nanoparticle, shown in Fig. 2b. From the magnified HRTEM image of the selected area (inset of Fig. 2b), the lattice fringes could be observed clearly and the lattice spacing was 0.362 nm, corresponding to the (012) plane of α-Fe_2O_3. In comparison, the Cu doped α-Fe_2O_3 (α-$Fe_{1.92}Cu_{0.08}O_3$) particles with a mean particle size of ~40 nm showed monodispersity (see Fig. 2c). The corresponding HRTEM image (Fig. 2d) displays the (104) plane with the d spacing of 0.266 nm for α-$Fe_{1.92}Cu_{0.08}O_3$. However, the d spacing did not increase significantly as expected, comparing with the value of undoped α-Fe_2O_3. TEM analysis of α-$Fe_{2-x}Cu_xO_3$ nanoparticles is comparable to that of the Cu-doped α-Fe_2O_3 cubes reported in Sun's study.[11]

3.2. Structural characteristics of the α-$Fe_{2-x}Cu_xO_3$ nanoparticles

The XRD patterns of the α-$Fe_{2-x}Cu_xO_3$ nanoparticles are shown in Fig. 3a. For undoped α-Fe_2O_3, all the diffraction peaks can be indexed by a single phase with the rhombohedral crystal structure of α-Fe_2O_3, which is consistent with the standard data file (PDF # 033-0664). For the α-$Fe_{2-x}Cu_xO_3$ ($0 < x \leq 0.17$)

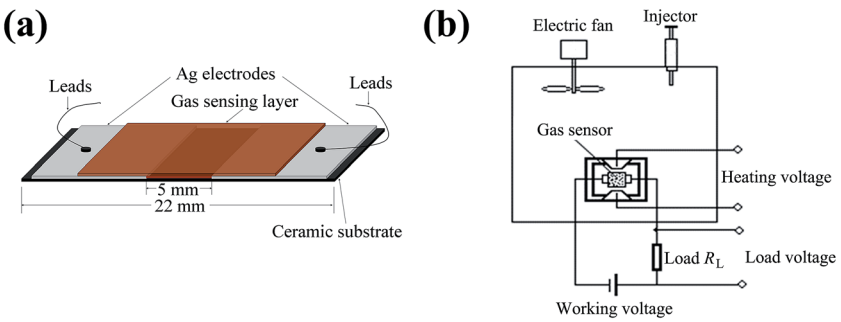

Fig. 1 Schematic of (a) α-$Fe_{2-x}Cu_xO_3$ gas sensors and (b) equipment for the sensor response measurements.

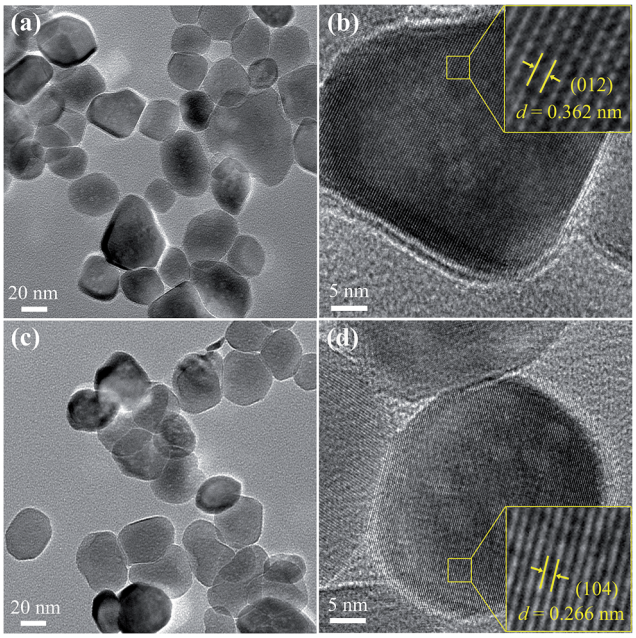

Fig. 2 TEM images of α-$Fe_{2-x}Cu_xO_3$ nanoparticles: (a) bright field TEM image and (b) HRTEM image showing grain with the (012) plane of undoped α-Fe_2O_3, (c) bright field TEM image and (d) HRTEM image showing grains with the (104) plane of α-$Fe_{1.92}Cu_{0.08}O_3$.

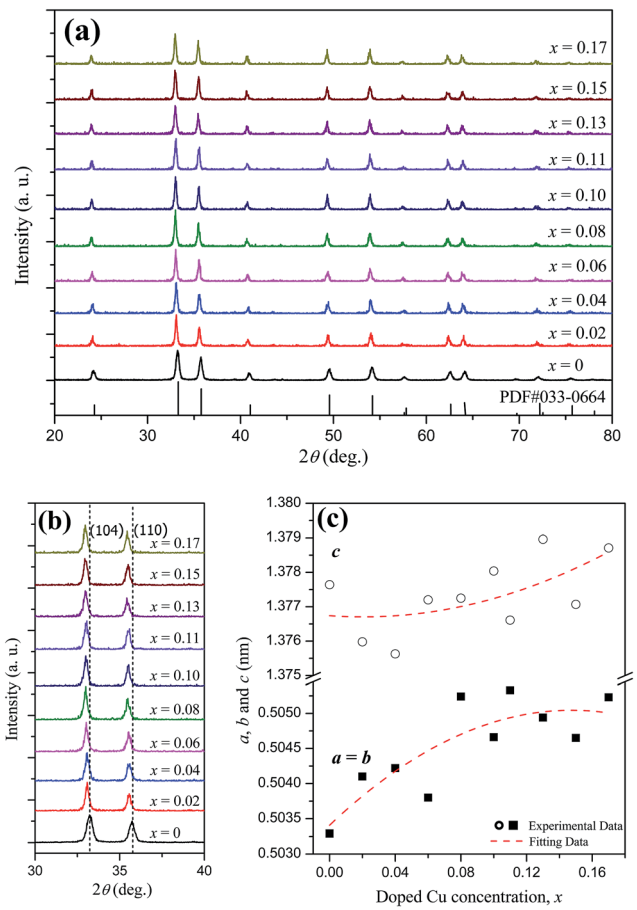

Fig. 3 (a) XRD patterns, (b) zoomed-in (104) and (110) peaks, and (c) room-temperature lattice parameters of α-$Fe_{2-x}Cu_xO_3$ nanoparticles.

nanoparticles, all diffraction peaks can also be successfully indexed to rhombohedral hematite and no other evident trace of impurity phase particularly copper oxide is detected. This indicates that the added Cu could be doped into the crystal structure of α-Fe_2O_3, retaining the rhombohedral structure of hematite. Furthermore, from the zoomed-in (104) and (110) diffraction peaks of the α-$Fe_{2-x}Cu_xO_3$ nanoparticles, as seen in Fig. 3b, the diffraction peaks all shifted to lower 2θ angles compared to those of undoped α-Fe_2O_3, and the offset of peaks increased with increasing doped Cu concentration. To investigate the effects of doped Cu on the crystal structure of α-Fe_2O_3, the room-temperature lattice parameters of α-$Fe_{2-x}Cu_xO_3$ nanoparticles were obtained by the software X'Pert HighScore Plus based on the XRD data, as depicted in Fig. 3c. The results show that the lattice parameters a, b and c, all increased with increasing doped Cu concentration. The ionic radii (six-coordination in a rhombohedral structure) of Fe^{3+} and Cu^{2+} are similar at 0.0645 nm and 0.073 nm,[13] respectively. Therefore, Cu^{2+} can be doped into the crystal structure of α-Fe_2O_3 and partly substitute Fe^{3+}. There is no doubt that the lattice parameters may increase when the substitutions exist. Hence, the shift of diffraction peaks and increase in lattice parameters are in association with the substitutions of Fe^{3+} by Cu^{2+}. In addition, with increasing doped Cu concentration (x), the lattice parameters of α-$Fe_{2-x}Cu_xO_3$ increased gradually, which was accompanied by the shift of the diffraction peaks to lower 2θ angles.

In addition, to further investigate the structural distortion of Cu-doped α-Fe_2O_3 nanoparticles, the Raman spectra of the α-$Fe_{2-x}Cu_xO_3$ nanoparticles at room temperature were collected (see Fig. 4). The Raman peaks located at 222 cm^{-1} and 493 cm^{-1} correspond to A_{1g} modes, whereas the peaks at 241 cm^{-1}, 289 cm^{-1}, 405 cm^{-1}, and 606 cm^{-1} are assigned to E_g modes. This confirms the corundum structure of α-$Fe_{2-x}Cu_xO_3$ ($0 \leq x \leq 0.17$), which is consistent with the values reported in the literature.[14,15] In general, substitutions of larger ions at the Fe sites may lead to an increase in the mean Fe–O bond length, resulting in a shift of the Raman peaks to lower wavenumbers. However, in the present study, it is puzzling that all of the Raman peaks of Cu doped α-Fe_2O_3 shifted slightly to higher wavenumbers, compared to those of undoped α-Fe_2O_3. According to Yogi and Varshney, similar Raman spectrum changes were also observed and attributed to the strong electron–phonon interactions and structural distortion in this system after doping Cu, accompanied with an increase in chemical bond strength.[14] These structural changes of the α-$Fe_{2-x}Cu_xO_3$ nanoparticles induced by doped Cu are expected to have an effect on the electrical and CH_4 sensing properties.

3.3. Electrical properties of the α-$Fe_{2-x}Cu_xO_3$ gas sensors

Fig. 5 shows the conductivities of the α-$Fe_{2-x}Cu_xO_3$ gas sensors at room temperature. The conductivities of the sensors were calculated using eqn (1):

$$\sigma = \frac{1}{\rho} = \frac{L}{RS} \quad (1)$$

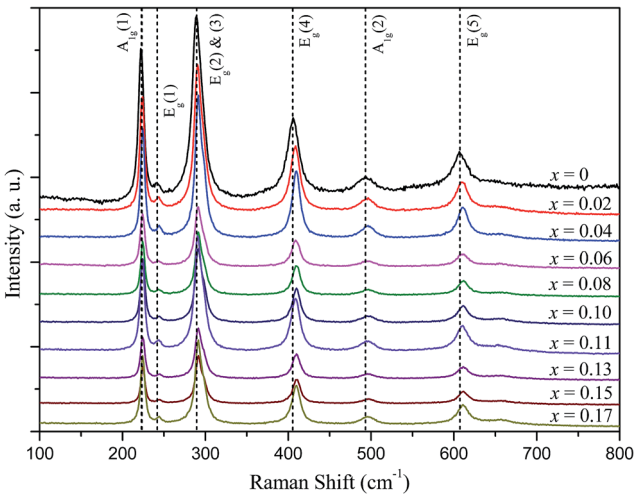

Fig. 4 Raman spectra of α-$Fe_{2-x}Cu_xO_3$ nanoparticles at room temperature.

where σ is the conductivity, ρ is the resistivity, L is the distance of the Ag electrodes, R is the resistance of α-$Fe_{2-x}Cu_xO_3$ gas sensor and S is the cross-sectional area of α-$Fe_{2-x}Cu_xO_3$ layer. As shown in Fig. 5, the conductivity of the α-$Fe_{2-x}Cu_xO_3$ gas sensor increased from 1.2×10^{-5} to 6.3×10^{-5} S m^{-1} with increasing x in α-$Fe_{2-x}Cu_xO_3$ from 0 to 0.17. Clearly, Cu doping enhances the electric conduction capability of α-Fe_2O_3 gas sensor greatly.

According to Long's research,[16] α-Fe_2O_3 annealed in air is an n-type semiconductor and the one annealed in oxygen usually a p-type semiconductor because a large amount of metallic ionic vacancies (point defects) will be formed if annealed in an oxygen atmosphere. These metallic ionic vacancies can accept electrons, and the holes are the majority carriers in α-Fe_2O_3 semiconductor material. For Cu doped α-Fe_2O_3, when a part of Fe^{3+} sites are occupied by Cu^{2+}, holes with a +1 charge are formed simultaneously. This will no doubt increase the concentration of hole carriers and enhance the conductivity of the p-type α-Fe_2O_3 semiconductor. On the other hand, acceptor energy level (usually called isolated energy level) can be introduced between the valence band and conduction band if the substitutions of Cu^{2+} ions occur at the Fe sites. The acceptor impurities on the acceptor energy level will ionize and lead to an increase in conductive holes in the valence band. As a result, the conduction capability of the Fe_2O_3 semiconductor is enhanced, and the conductivity of the α-$Fe_{2-x}Cu_xO_3$ sensor increases with increasing doped Cu concentration.

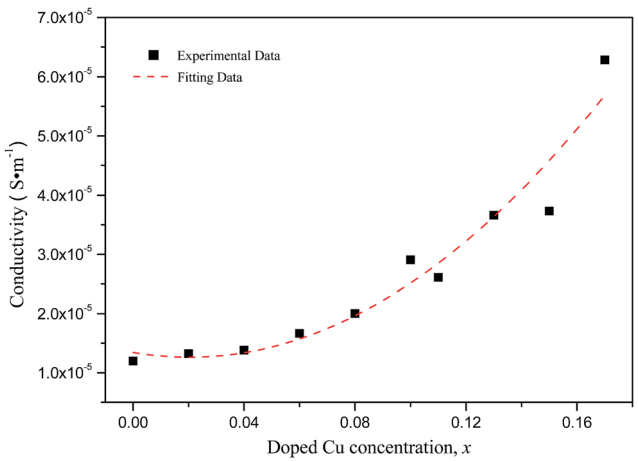

Fig. 5 Conductivities of α-$Fe_{2-x}Cu_xO_3$ gas sensors at room temperature.

3.4. CH_4 sensing properties of the α-$Fe_{2-x}Cu_xO_3$ gas sensors

Fig. 6 depicts CH_4 gas response of the α-$Fe_{2-x}Cu_xO_3$ gas sensors in an atmosphere containing CH_4 (2000 ppm) at 25 °C and 50% relative humidity (RH); the inset shows the gas response of the undoped α-Fe_2O_3 and α-$Fe_{1.92}Cu_{0.08}O_3$ gas sensors to CH_4 with different concentrations at 25 °C and 50% RH. The undoped α-Fe_2O_3 nanoparticles have a lower response to 2000 ppm CH_4 gas at room temperature. In contrast, the response of the α-$Fe_{2-x}Cu_xO_3$ ($0 < x \leq 0.17$) gas sensor is significantly higher at room temperature and at the same concentration of CH_4 gas. The maximum response to 2000 ppm CH_4 at room temperature was obtained when x in α-$Fe_{2-x}Cu_xO_3$ $\approx$ 0.10. Although the maximum response is only ~1.06, this material is also a potential candidate for methane gas sensor applications because the working temperature is much lower in the present case. The sensor using α-$Fe_{2-x}Cu_xO_3$ nanoparticles as gas sensing material exhibits a receivable response to CH_4 at room temperature. The inset in Fig. 6 indicates that the response increased almost linearly with increasing concentration of CH_4 gas from 500 to 4000 ppm, meeting the common requirements in application.

Moreover, for environmental monitoring of methane emissions at room temperature, the selectivity of the α-$Fe_{2-x}Cu_xO_3$ gas sensors was also evaluated. Fig. 7a shows the response of the α-$Fe_{2-x}Cu_xO_3$ gas sensors to different test gases (1000 ppm), *i.e.*, CO_2, C_2H_5OH and NH_3, at 25 °C and 50% RH. In the CO_2

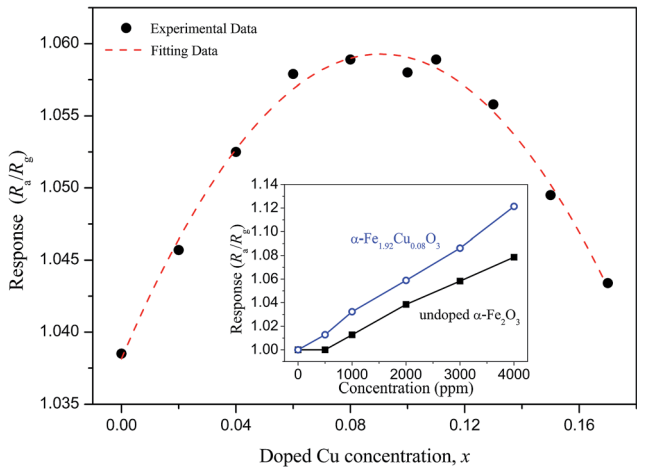

Fig. 6 CH_4 gas response of the α-$Fe_{2-x}Cu_xO_3$ gas sensors in an atmosphere containing CH_4 (2000 ppm) at 25 °C and 50% RH. The inset shows the gas response of undoped α-Fe_2O_3 and α-$Fe_{1.92}Cu_{0.08}O_3$ gas sensors to CH_4 with different concentrations at 25 °C and 50% RH.

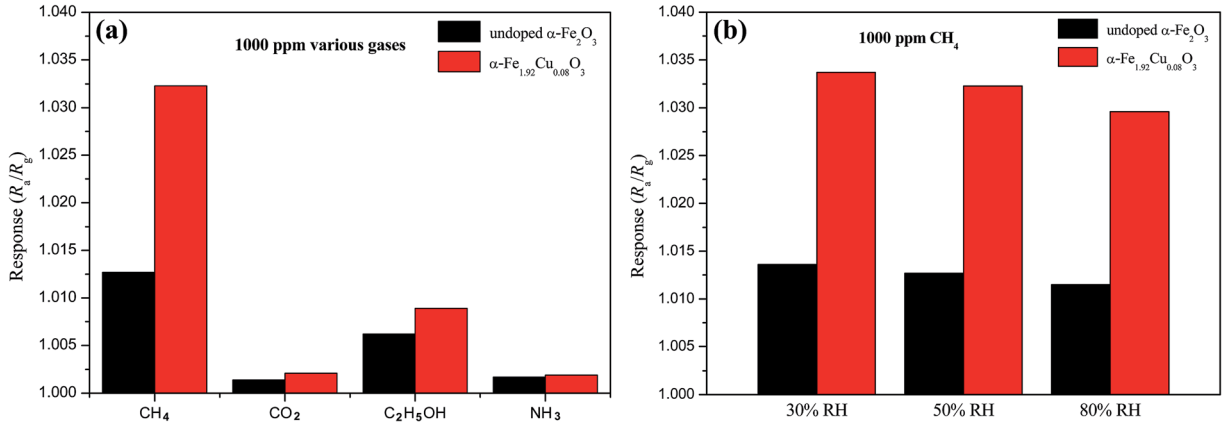

Fig. 7 (a) Response of the α-$Fe_{2-x}Cu_xO_3$ gas sensors to different test gases at 25 °C and 50% RH. (b) Effect of humidity on the sensor response to 1000 ppm CH_4 at 25 °C.

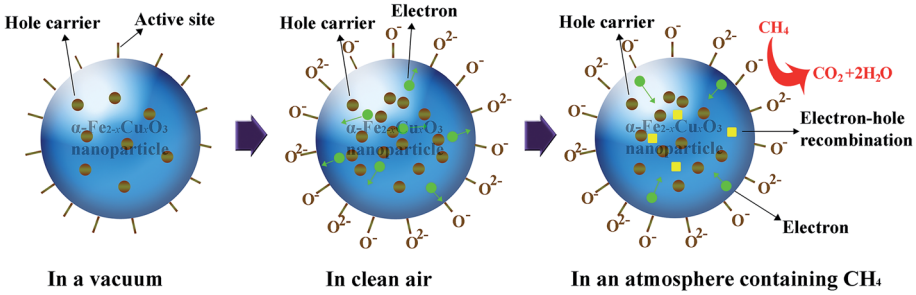

Fig. 8 Schematic explaining the methane sensing mechanism of α-$Fe_{2-x}Cu_xO_3$ nanoparticles.

sensing testing, only 700 ppm CO_2 was injected because clean air contains around 300 ppm CO_2. This shows that the response of the sensors to CH_4 is the highest, indicating that the α-$Fe_{2-x}Cu_xO_3$ sensor has good selectivity for CH_4, even though it exhibits a certain response to C_2H_5OH. As expected, Cu doping can significantly improve the selectivity of the sensor for CH_4. Fig. 7b displays the effect of humidity on the sensor response at 25 °C. Water vapors in the atmosphere had an evident effect on the performance of the α-$Fe_{2-x}Cu_xO_3$ sensor; the response to CH_4 was higher in dryer air than in a humid environment. The adsorption of water affects the electronic properties of α-$Fe_{2-x}Cu_xO_3$, usually acting as a donor. Thus, long exposure in a humid environment can lead to hydration of the surface layer, and a corresponding drift of the sensor performance.[17] However, avoiding or mitigating the impact of water vapor is a major problem for gas sensors working at room temperatures. Although some coatings, for example, Teflon, have been used to either consume water vapor or permit the passage of selected gases to the sensor,[18] further related research is needed.

The CH_4 sensing mechanism (depicted in Fig. 8) of α-$Fe_{2-x}Cu_xO_3$ nanoparticles is a surface controlled process and can be understood as follows. In vacuum, there are a great number of unstable active sites on the surface of the p-type α-$Fe_{2-x}Cu_xO_3$ semiconductor, with holes as majority carriers. When α-$Fe_{2-x}Cu_xO_3$ nanoparticles are exposed to air, a certain amount of oxygen from the air is adsorbed on the surface of α-$Fe_{2-x}Cu_xO_3$ in the form of O_2^- or O^-, by transferring electrons from the conduction band to the adsorbed oxygen atoms. In this process, the formation of chemisorbed oxygen species results in a decrease in the free electron concentration in the material conduction band. Consequently, the conductivity of the p-type semiconductor will increase.[10,11] It should be noted that the amount of chemisorbed oxygen species may be affected, even decreased, with the increasing adsorption of water vapor on the surface of α-$Fe_{2-x}Cu_xO_3$, which is not conducive to improving the gas sensing performance. Once the α-$Fe_{2-x}Cu_xO_3$ nanoparticles are exposed to an atmosphere containing CH_4, surface reaction between the adsorbed oxygen species and CH_4 molecules will occur, resulting in the release of electrons trapped in the ionized oxygen species back into the materials and electron–hole recombination, thereby decreasing the concentration of hole carriers and lowering the measured conductivity.

4. Conclusion

α-$Fe_{2-x}Cu_xO_3$ ($0 \leq x \leq 0.17$) nanoparticles were synthesized by an improved homogenous co-precipitation method. The morphological and structural characteristics showed that α-$Fe_{2-x}Cu_xO_3$ ($0 < x \leq 0.17$) nanoparticles with an average particle size of ~40 nm also have a single phase with a rhombohedral

corundum structure. Owing to the substitution of Cu^{2+} at Fe^{3+} sites, the lattice parameters of α-$Fe_{2-x}Cu_xO_3$ increase with increasing doped Cu concentration. The shift of Raman peaks for α-$Fe_{2-x}Cu_xO_3$ to higher wavenumbers was observed due to the strong electron–phonon interaction and structural distortion after doping Cu. Doping Cu can also increase the concentration of hole carriers and enhance the conductivity of p-type α-Fe_2O_3 semiconductor. The CH_4 sensing characterization show that the α-$Fe_{2-x}Cu_xO_3$ nanoparticles are sensitive and have good selectivity to CH_4 at room temperature, and the response of the α-$Fe_{2-x}Cu_xO_3$ ($0 < x \leq 0.17$) gas sensor is significantly improved by doping Cu. The maximum response to 2000 ppm CH_4 at room temperature and 50% RH was obtained when x in α-$Fe_{2-x}Cu_xO_3$ $\approx$ 0.10, meeting the common requirements in application. Based on these results, the α-$Fe_{2-x}Cu_xO_3$ ($0 < x \leq 0.17$) nanoparticles can be considered potential candidates for methane detection at room temperature.

Acknowledgements

This study was supported by the National Natural Science Foundation of China (grant number 51502249); the Scientific Research Fund of Education Department of Sichuan Province (grant numbers 16ZA0133 and 15ZB0108); and the Doctoral Foundation of Southwest University of Science and Technology (grant number 15zx7105).

References

1 J. Hill, C. McSweene, A. D. G. Wright, G. Bishop-Hurley and K. Kalantar-zadeh, *Trends Biotechnol.*, 2016, **34**, 26.
2 Z. K. Horastani, S. M. Sayedi, M. H. Sheikhi and E. Rahimi, *Mater. Sci. Semicond. Process.*, 2015, **35**, 38.
3 A. Das, V. Bonu, A. K. Prasad, D. Panda, S. Dhara and A. K. Tyagi, *J. Mater. Chem. C*, 2014, **2**, 164.
4 T. Sarangi, M. Naja, S. Lal, S. Venkataramani, P. Bhardwaj, N. Ojha, R. Kumar and H. C. Chandola, *Atmos. Environ.*, 2016, **125**, 450.
5 S. Maduskar, A. R. Teixeira, A. D. Paulsen, C. Krumm, T. J. Mountziaris, W. Fan and P. J. Dauenhauer, *Lab Chip*, 2015, **15**, 440.
6 J. A. Sinclair, P. G. J. Irwin, S. B. Calcutt and E. L. Wilson, *Icarus*, 2015, **260**, 103.
7 B. Dong, Z. Han, Y. B. Zhang, Y. Y. Yu, A. G. Kong and Y. K. Shan, *Chem.–Eur. J.*, 2016, **22**, 2046.
8 J. Hu, F. Q. Gao, Z. T. Zhao, S. B. Sang, P. W. Li, W. D. Zhang, X. T. Zhou and Y. Chen, *Appl. Surf. Sci.*, 2016, **363**, 181.
9 S. M. Sedghi, Y. Mortazavi and A. Khodadadi, *Sens. Actuators, B*, 2010, **145**, 7.
10 A. Amutha, S. Amirthapandian, A. K. Prasad, B. K. Panigrahi and P. Thangadurai, *J. Nanopart. Res.*, 2015, **17**, 289.
11 P. Sun, C. Wang, X. Zhou, P. F. Cheng, K. Shimanoe, G. Y. Lu and N. Yamazoe, *Sens. Actuators, B*, 2014, **193**, 616.
12 H. F. Liu, T. J. Peng, H. J. Sun, L. Fan and B. G. Guo, *Adv. Mater. Res.*, 2010, **96**, 105.
13 R. D. Shannon, *Acta Crystallogr.*, 1976, **32**, 751.
14 A. Yogi and D. Varshney, *Mater. Sci. Semicond. Process.*, 2014, **21**, 38.
15 L. Kopanja, I. Milosevic, M. Panjan, V. Damnjanovic and M. Tadic, *Appl. Surf. Sci.*, 2016, **362**, 380.
16 N. V. Long, Y. Yang, M. Yuasa, C. M. Thi, Y. Cao, T. Nann and M. Nogami, *RSC Adv.*, 2014, **4**, 8250.
17 A. Mirzaei, B. Hashemi and K. Janghorban, *J. Mater. Sci.: Mater. Electron.*, 2016, **27**, 3109.
18 S. Yamaguchi, *Mater. Chem.*, 1981, **6**, 505.